

Advanced Evaporators for Lunar Lander and Lunar Habitat Thermal Control Applications

Tadej Semenic

*Advanced Cooling Technologies, Inc.
1046 New Holland Avenue
Lancaster, PA 17601
717-295-6061; Tadej.Semenic@1-ACT.com*

Abstract. Six 20.3cm x 20.3cm (8in x 8in) evaporators for Lunar Lander and Lunar Habitat thermal control applications were designed, fabricated and tested in a vapor compression loop at heat loads in the range of 3-6 kW. The evaporator heated area was 826cm² and their total mass ranged from 1.0kg to 3.2kg depending on the design. The primary objective of the study was to investigate different evaporator designs and identify and characterize the evaporator design with the lowest temperature, most uniform temperature, smallest mass, and lowest pressure drop. The results obtained using serpentine evaporators showed excellent temperature uniformity ($\pm 3^{\circ}\text{C}$) across the evaporator surface at these relatively high heat loads. The temperature lift from the evaporator surface to the average condenser coolant temperature was also measured and ranged from 30 to 50°C depending on the heat load. The Coefficient of Performance (COP), defined as the ratio of the heat load to the compressor work at 6kW, was 1.9. The best evaporator out of six evaporators tested transferred heat at one half of the thermal resistance of the baseline evaporator, while maintaining the same system COP.

Keywords: Lunar Lander thermal control, serpentine evaporators, mini-channel evaporators, two-phase cold plates, high temperature lift vapor compression, two-phase refrigeration cooling

PACS: 44.35c Heat flow in multiphase systems

INTRODUCTION

In support of NASA's vision for space exploration, the Altair Lunar Lander is being developed to enable four astronauts to land on the moon and provide them with life support and a base for surface exploration missions. To support the mission, advanced Thermal Control Systems (TCS) are required to maintain cabin and electronic temperatures within acceptable levels. This poses unique challenges especially taking into consideration the fact that the lunar surface temperature ranges from less than -173°C on the dark side to as high as 127°C in the vicinity of subsolar point (Stephan, 2009). Furthermore, the lunar surface temperature at the equator varies widely from -173°C to 121°C over the course of the lunar day (28 Earth days) (Swanson *et al.*, 1990).

The temperature of the TCS for the Lunar Surface System (LSS) is further expected to be about 0°C while the maximum heat sink temperature at the lunar equator is known to be around 47°C at lunar noon (Ewert, 1993). Thus, a temperature lift of 50°C (or more) will be required to reject the waste heat from the surface systems to the heat sink. To meet this requirement, several TCS technologies have been considered (Simonson and DeBarro, 1988) where the most promising options are heat pumps (Sridhar and Gottmann, 1996) that use electrical energy to remove excess heat from a lower temperature source to a higher temperature radiator. The waste heat is then radiated into space.

Technically, the most advanced heat pumps rely on the Rankine or vapor compression loop (VCL) and are highly effective and reliable. As such, advanced VCL should be considered for thermal control of the Lunar Landers and Lunar Habitats as they offer high temperature lift and reliable operation at various locations on the lunar surface and at different times during the lunar day.

Therefore, an advanced vapor compression system for high temperature lift has been developed at Advanced Cooling Technologies, Inc. (ACT) and is currently being used to test advanced evaporators at conditions that are representative of those that will be encountered in the Lunar Lander and LSS. The primary components of the loop include an evaporator, a compressor, a condenser, and an expansion valve. In addition, however, several secondary components have been added to the loop to further improve the system performance and safety. These include: a recuperating heat exchanger (recuperator), a two-phase separator upstream of the evaporator and an oil separator located at the compressor outlet.

An overview of the VCL test bed and its components is described in this paper with a special focus on the modeling, design, fabrication and testing of advanced evaporators. Both serpentine and parallel-channel evaporators have been designed and developed including several advanced serpentine evaporators that incorporate a twisted tape and/or a wick for improving the internal distribution of the two-phase mixture. Data on the performance of the evaporator and the VCL is also presented and all results are compared to baseline data acquired with the serpentine evaporator. This comparison provides a quantitative basis by which to evaluate the performance of the different evaporator designs. The objective of this study was to identify the evaporator design with the lowest and the most uniform evaporator temperature, the lowest evaporator mass, and the lowest evaporator pressure drop.

Six evaporators were designed and fabricated. All the evaporators were tested at different heat loads with and without liquid-vapor phase separation upstream of the evaporator inlet. Test results demonstrate excellent temperature uniformity ($\pm 3^\circ\text{C}$) across the evaporator surface for heat loads in the range of 4-6kW. The best evaporator transferred heat at one half of the thermal resistance of the baseline evaporator. The compressor power consumption for the best evaporator was the same as for the baseline evaporator. The temperature lift from the evaporator wall to the average condenser coolant temperature was also measured and ranged from 30 to 50°C depending on the heat load. In all tests, a relatively small evaporator area of 826cm² (for heating on both sides of the evaporator) was chosen to maximize the evaporator heat flux and to determine the limiting heat flux for each evaporator design. It is however recognized that the evaporator area may be larger in the Lunar Lander or Lunar Habitat TCS depending on the required surface area for mounting electronics components.

EVAPORATOR DESIGN

Based on the flow configuration, different types of evaporators have been developed for VCL and are generally either serpentine channel or parallel channel configurations. In serpentine channel evaporators, the refrigerant flows through a single tube or a channel in contrast to parallel channel evaporators where the refrigerant is distributed among multiple tubes or channels. On one hand, parallel channel evaporators are typically more compact than serpentine channel evaporators, yet may suffer from non-uniform distributions in the mass flow rate and refrigerant vapor quality in adjacent channels, which in turns adversely affects the temperature uniformity and may cause system instabilities and adverse flow of the vapor.

It is therefore critically important that the geometry of the evaporator be optimized for the particular application. As such, a thermodynamic model of the VCL was developed for application to LSS and used to predict pressures and temperatures at different locations along the loop. An evaporator model was also developed and used to compute the two-phase pressure drop and heat transfer associated with different evaporators designs. For these calculations, it was decided to use a homogeneous equilibrium model to calculate the pressure drops and a generalized form of Chen's model (Chen, 1963; Zhang *et al.*, 2004) to compute two-phase heat transfers. Several other models were also considered.

Evaporator Model

The loop thermodynamic model was used to compute the inlet conditions to the evaporator (i.e., pressure, temperature, vapor quality), and refrigerant mass flow rate, which was then used in the evaporator model to calculate the evaporator wall temperature and evaporator outlet conditions. In the model, the evaporator length was divided into n segments each with a length dz . For a given evaporator wall heat flux, q_w , and evaporator hydraulic diameter, d_h , the local vapor quality at the outlet of the $i+1^{st}$ segment, x_{i+1} , was calculated as

$$x_{i+1} = x_i + \frac{4q_w}{Gd_h} \frac{dz}{h_{fg}(T_{sat,i})} \quad (1)$$

where $h_{fg}(T_{sat,i})$ is the latent heat of vaporization, and G is the mass flux. Knowing the vapor quality, the following equation was used to compute the two-phase pressure drop for an evaporator with a length, L (Agostini, *et al.*, 2008)

$$\Delta p_{tp} = \int_0^L \left[\left(\frac{2f_{tp}G^2}{d_h\rho_{tp}} \right)_f + G^2 \left((v_g - v_l) \cdot \frac{dx}{dz} + x \frac{dv_g}{dp} \cdot \left(\frac{2f_{tp}G^2}{d_h\rho_{tp}} \right)_a \right) \right] dz \quad (2)$$

The first group of terms in parenthesis is the two-phase friction pressure drop and the second group is the acceleration pressure drop. The other parameters in Equation (2) include: f_{tp} , the two-phase friction factor; ρ_{tp} , the two-phase density; v_g , the specific volume of vapor; and v_l , the specific volume of liquid. A correlation was also developed to evaluate dv_g/dp as a function of local pressure.

To model the two-phase flow heat transfer, the model reported by Zhang *et al.* (2004) was used. The model is based on Chen's (1963) model and predicts the two-phase heat transfer coefficient (h_{tp}) as a function of vapor quality and assumes the following form

$$h_{tp} = S \cdot \left[0.00122 \left(\frac{k_f^{0.79} c_{pf}^{0.45} v_g^{0.24}}{\sigma^{0.5} \mu_f^{0.29} h_{fg} v_f^{0.49}} \right) \Delta T_{sat}^{0.24} \Delta p_{sat}^{0.75} \right] + F \cdot h_{sp} \quad (3)$$

where S and F are the suppression and the Reynolds number factors introduced by Chen (1963), k_f is thermal conductivity of the liquid phase, c_{pf} is the specific heat of the liquid phase, σ is the surface tension, ΔT_{sat} is the difference between the wall temperature and the saturation temperature, Δp_{sat} is the difference between the pressure evaluated at the wall temperature and the saturation pressure, and h_{sp} is the single phase heat transfer coefficient for the liquid phase.

To validate the model, data from the literature (for example: Agostini *et al.*, 2008; Tran *et al.*, 1999; Kattan, 1998) was compared to the predicted pressure drops. The range of hydraulic diameters that were considered ranged from 0.3mm to 12.7mm, which includes both mini to macro-channels. In addition, the predicted heat transfer coefficient was compared to the measured values taken from Yu *et al.* (2002), Greco and Vanoli (2005), and Agostini *et al.* (2008) for hydraulic diameters ranging from 0.3mm to 10.7mm. Comparisons of the experimental and predicted pressure drops and heat transfer coefficients, h_{tp} are shown in Figure 1.

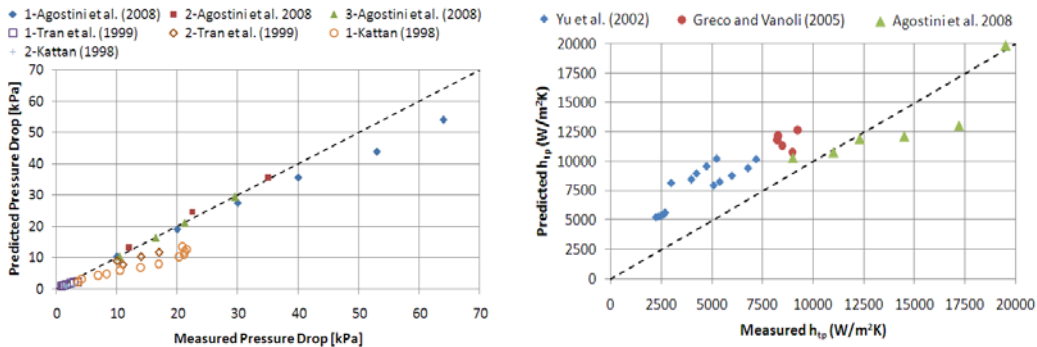


FIGURE 1: Comparison between predicted and measured pressure drops and heat transfer.

It can be seen from Figure 1 that the predicted pressure drop agrees with measured data within $\pm 25\%$ while the heat transfer coefficients are over-predicted by an average of 60%. These predictions are within acceptable levels (Sun and Mishima, 2009).

As mentioned, six different evaporator designs were considered including a serpentine evaporator with a twisted tape. The different designs are discussed in the next section, yet here it should be noted that for the evaporators with the twisted tape, the two-phase friction factor for a smooth tube was replaced with the friction factor for fully developed turbulent flow for tubes with twisted tapes from Abu-Khader (2006):

$$f_{tp} = \frac{0.0791}{Re_{tp}^{0.25}} \left(\frac{\pi}{\pi - 4\delta/d_h} \right)^{1.75} \left(\frac{\pi + 2 - 2\delta/d_h}{\pi - 4\delta/d_h} \right)^{1.25} \left(1 + \frac{2.752}{y^{1.29}} \right) \cdot \left(\frac{\eta_{sat}}{\eta_w} \right)^{-0.14} \quad (4)$$

where Re_{tp} is the two-phase Reynolds number, δ is the twisted tape thickness and, y is the twisted tape ratio defined as the ratio of the twist pitch and the hydraulic diameter, and η_{sat} and η_w are two-phase viscosities evaluated at the saturation and the wall temperature, respectively. Similarly, the single phase heat transfer coefficient in Equation (3) was obtained using the following correlation developed for fully developed turbulent flow for tubes with twisted tapes (Manglik and Bergles, 1993)

$$Nu = 0.023 Re^{0.8} Pr^{0.4} \left(\frac{\pi}{\pi - 4\delta/d_h} \right)^{0.8} \left(\frac{\pi + 2 - 2\delta/d_h}{\pi - 4\delta/d_h} \right)^{0.2} \cdot \left(\frac{\eta_{sat}}{\eta_w} \right)^{0.18} \quad (5)$$

The evaporator models were integrated with the loop thermodynamic model and used to compute the evaporator wall temperature and evaporator pressure drop. The models were the used to perform tradeoff studies of different evaporator types with different hydraulic diameters.

Evaporator Designs

The evaporator model was used together with the Finite Element Analysis modeling tools SolidWorks and Cosmos Works to design seven different evaporators:

- Evaporator 1 (E1): Serpentine Evaporator
- Evaporator 2 (E2): Serpentine Evaporator with Twisted Tape
- Evaporator 3 (E3): Serpentine Evaporator with Wick
- Evaporator 4 (E4): Serpentine Evaporator with Wick and Twisted Tape
- Evaporator 5 (E5): Parallel Channel Evaporator (with circular channels)
- Evaporator 6 (E6): Three-Pass Minichannel Evaporator (with rectangular channels)

The evaporator model was used to optimize the channel hydraulic diameter and to minimize the evaporator thermal resistance and pressure drop. Several design options were also considered to minimize the total evaporator mass. The evaporator geometry and spacing between channels was then modeled with SolidWorks and a stress analysis was performed with Cosmos Works to ensure a sufficient safety factor.

In addition to minimizing the thermal resistance, pressure drop and mass of the evaporators, special attention was given to ensure that the operation of the evaporators was gravity-independent. The following input parameters were used to the evaporator model for all of the evaporator designs:

- Evaporator geometries should be flat/ planar with an 20.3cm x 20.3cm footprint
- Evaporator heat loads of 4000W (2000W on each evaporator side)
- The condensing temperature for the refrigerant was 45°C
- Superheating of the refrigerant occurs in the recuperating heat exchanger (liquid suction heat exchanger)

In the following sections, the different evaporator designs are reviewed starting with the serpentine tube evaporators with and without twisted tapes and/or wicks. Following are parallel channel evaporator and three-pass minichannel evaporator.

Serpentine Tube Evaporators: E1, E2, E3, and E4

Evaporator 1: Evaporator E1 is a serpentine tube evaporator that contains eight passes with an inlet and an outlet on the same side. Different tube hydraulic diameters along with different numbers of turns (passes) were considered in the design process. A summary of the predicted performances of the E1 evaporator design for different hydraulic diameters, d_h , is given in Table 1. Vapor inlet quality and mass flow rate were determined to be 17% and 0.023kg/sec, respectively.

Table 1. Selected E1 design options.

Hydraulic Diameter (cm)	Evaporator Thickness (cm)	Wall Heat Flux (W/cm ²)	Inner Wall Temperature (°C)	Pressure Drop (Pa)
1.7	2.5	4.5	-1.5	2068
1.4	2.2	5.6	-0.9	4826
1.1	1.9	7.2	0.1	13100
0.8	1.6	10.1	3.1	53779

After considering the design options, a hydraulic diameter of 1.4cm was selected. Hydraulic diameters smaller than 1.4cm was not chosen due to the high computed pressure drop (see Table 1) while an evaporator diameter larger than 1.4cm was not feasible due to a small tube bending radius for a 2.5cm tube spacing. The serpentine evaporator was then constructed by joining eight 22.9cm long straight copper tubes with pairs of 90 degree copper elbows. Two aluminum saddle-shape plates 20.3cm x 20.3cm were fabricated to a high tolerance and clamped around the serpentine tube as shown in Figure 2. The evaporator thickness was 2.2cm and the computed evaporator mass was 2.5kg.

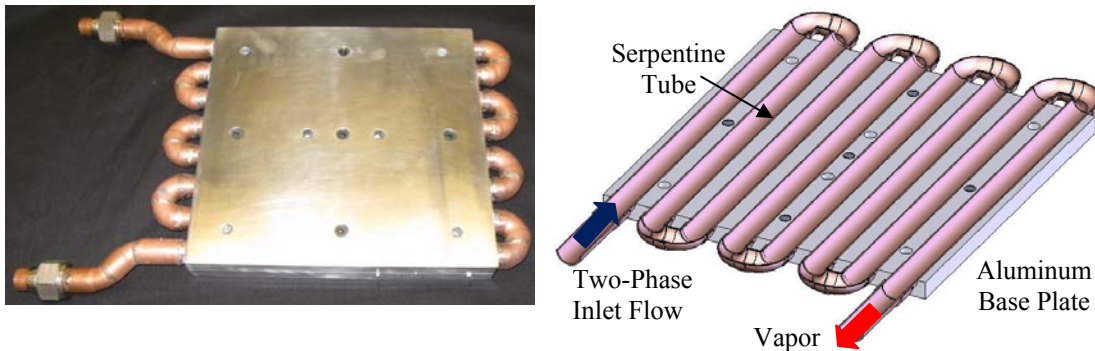


FIGURE 2. Evaporator 1 design (left) and section view (right).

Evaporator 2: The second serpentine evaporator, E2, was identical to E1 yet included twisted tape inserts. The purpose of the twisted tape is to create a tangential swirl in the evaporator to aide separation of the liquid and the vapor phases. In response to the centrifugal acceleration, the denser liquid phase accumulates on the evaporator wall while the less dense vapor collects in the evaporator core.

A study of the different twisted tape designs considered is summarized in Table 2 where the results for a baseline evaporator E1 are listed in the first row for comparison.

The results show that adding a twisted tape increases evaporator pressure drop, but reduces the evaporator wall temperature. No significant difference in wall temperature was predicted for twisted tapes with twist ratios between 1.8 to 4.1; therefore, a twisted tape with a twist ratio of 3.6 that had a pitch length (distance between the twisted tape nodes) of 5.1cm was selected. This particular twisted tape design was selected because it requires an even pitch length of 2.0 inches (5.1cm) and simplifies the fabrication. Note also that the tangential velocity listed in the third column increases as the twist ratio decreases.

Table 2. Selected twisted tape designs for evaporator E2

Pitch Length (cm)	Twist Ratio	Tangential Velocity (m/s)	Inner Wall Temperature (°C)	Pressure Drop (Pa)
N/A	N/A	0.0 (baseline)	-0.9 (baseline)	4,826 (baseline)
2.5	1.8	7.0	-3.2	12,411
3.2	2.3	5.6	-3.1	11,032
3.8	2.7	4.7	-3.1	10,342
4.4	3.2	4.0	-3.0	9,653
5.1	3.6	3.5	-3.0	9,653
5.7	4.1	3.1	-3.0	8,963

Comparing the performance of E2 with a twisted tape ratio of 3.6 with E1, we can see that E2 has $\sim 2^{\circ}\text{C}$ lower wall temperature albeit with a 4826Pa higher pressure drop. Dimensions for E2 are identical to those used in E1; however, the mass of E2 is slightly higher and predicted to be 2.8kg if the twisted tapes are fabricated from copper. The additional mass associated with the twisted tapes can however be significantly reduced with the use of lighter weight materials.

Evaporator 3: Evaporator E3 is similar to E1, yet includes a wick inside the straight sections of the serpentine tube. Based on subscale test results, a copper powder wick with a slightly tapered shape was used. The E3 design has a total mass of 2.9kg, which again can be reduced by potentially reducing the weight of the aluminum plates.

Evaporator 4: Evaporator E4 was also identical to E1, yet it included both a wick and a twisted tape inside in the straight sections of the evaporator. The diameter of the twisted tape in this design was 0.3cm smaller than that used in evaporator E2. The E4 design is shown in Figure 3 and has an estimated total mass of 3.2kg.

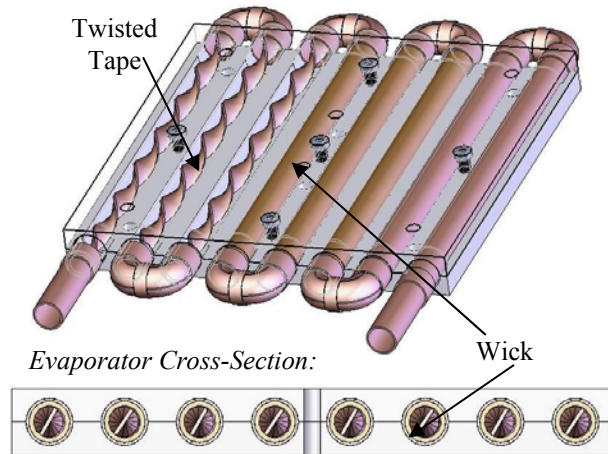


FIGURE 3. Section view of E4 design.

Parallel Channel Evaporators: E5 and E6

Evaporator 5: Evaporator E5 was a parallel channel evaporator with small circular channels that had a hydraulic diameter between that associated with macro- and mini-scale channels. After modeling different parallel channel designs, it was determined that 20 parallel channels with a channel hydraulic diameter of 0.6cm was the most appropriate for the 20.3cm x 20.3cm evaporator footprint. The model predicted that parallel channel evaporators with larger hydraulic diameter would result in lower evaporator wall temperature and will require fewer channels; however the total evaporator mass would be larger. It was decided to fabricate this evaporator design by drilling 20.3cm long holes into a solid aluminum block. A diameter of 0.6cm was found to be the smallest diameter that could be successfully drilled into the aluminum block. The inlet and outlet plenums were also designed to minimize the pressure drop in the plenums. The inlet plenum also included a narrow slit to prevent backflow of the vapor into the plenum. The inlet slit was also found to improve the flow distribution into the parallel channels and to assure that only the liquid phase entered the inlet plenum. Evaporator E5 was fabricated from aluminum with a thickness 1.3cm and mass of 1.3kg.

Evaporator 6: The final evaporator E6 is a multi-pass minichannel evaporator. This evaporator is a hybrid and combines parallel channels in a serpentine-type evaporator as shown in Figure 4.

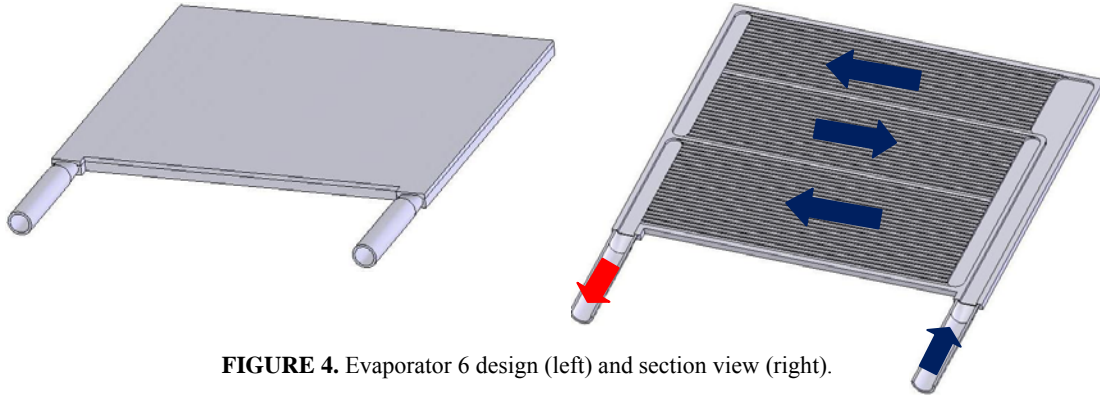


FIGURE 4. Evaporator 6 design (left) and section view (right).

After considering several design options, a three-pass serpentine, minichannel evaporator was selected. In this design, a two-phase mixture enters into the inlet plenum, flows across 16 parallel channels, turns in the outlet plenum and flows back to the inlet plenum across 18 channels, and subsequently returns to the outlet plenum by flowing through 23 channels. The velocity of the two-phase mixture increases as the liquid vaporizes resulting in an increase in pressure drop along the channel. In a way to minimize the pressure drop increase at the three evaporator sections, it was decided to increase the number of channels for each section. A summary of design options for E6 is shown in Table 3.

Based on the analysis, a channel width of 2.4mm and aspect ratio of one was selected. This evaporator will have a thickness of 0.95cm and mass of 1.1kg if fabricated from aluminum.

Table 3. Summary of design options for E6

Channel Width (mm)	Aspect Ratio	Wall Heat Flux (W/cm ²)	Evaporator Thickness (cm)	Inner Wall Temperature (°C)	Pressure Drop (Pa)
0.8	0.1	3.9	1.5	-1.4	44968
1.6	0.1	2.8	2.3	-3.6	3654
1.6	0.4	3.5	1.1	-3.2	11170
1.6	1	5	0.9	-0.4	55503
2.4	0.1	2.45	3.1	-3.8	965
2.4	0.2	2.6	1.9	-3.7	1448
2.4	0.6	3.5	1.1	-3.0	5171
2.4	1	4.4	1.0	-3.8	14962
3.2	0.2	2.5	2.3	-3.7	621
3.2	0.6	3.2	1.2	-3.1	2206

A summary of the evaporator thickness, mass and inner wall temperatures for the six evaporator designs is given in Table 4. While the parallel channel evaporators are the lightest, the results suggest that evaporators E4 (serpentine with twisted tape) and E6 (minichannel + serpentine) will have the lowest evaporator temperatures.

Summary of Trade-Offs in Evaporator Designs: Based on subscale tests with a single evaporator tube, we expect that evaporators E3 and E4 will result in lower evaporator temperatures than E2. Evaporators E2, E3, and E4 are also expected to have a higher pressure drop than the baseline evaporator E1 owed to the insertion of the twisted tape and the wick. The parallel and minichannel evaporators E5 and E6 will require single phase liquid at the evaporator inlet to improve flow distribution among the channels whereas the serpentine designs E1, E2, E3, and E4 are expected to be insensitive to inlet qualities. In terms of the evaporator mass, the parallel and minichannel evaporators E5 and E6 are significantly lighter than the serpentine tube evaporators; however, these may require phase separation upstream the evaporator which can increase the total mass of the system.

Table 4. Summary of six evaporator designs

Evaporator	Evaporator Thickness (cm)	Evaporator Mass (kg)	Inner Wall Temperature (°C)
Evaporator 1	2.2	2.5	-0.9
Evaporator 2	2.2	2.8	-3.1
Evaporator 3	2.2	2.9	/
Evaporator 4	2.2	3.2	/
Evaporator 5	1.3	1.3	0.1
Evaporator 6	1.0	1.1	-3.8

TEST BED

A VCL test bed was built that would enable the different evaporators to be easily installed and tested. The primary components of the test bed include the evaporator, a compressor (Maneurop MTZ064-3), a condenser (Flatplate FP5x12-40), and an expansion valve (SEI-2 electronic expansion valve with a Sporlan superheat controller). In addition, secondary components that include a two-phase flow separator and a recuperating heat exchanger (Flatplate SC-2G-5x13-12) were added to the test bed to evaluate their effect on the system performance and the evaporator temperature uniformity. In addition, a hot vapor by-pass line, a filter/drier, an oil separator (Temprite 900) located at the compressor outlet, and temperature and pressure sensors were also installed.

The pressure measurements on the low pressure side had an accuracy of ± 2.8 kPa (Omega PX603-100G) and the pressures on the high pressure side had an accuracy of ± 5.2 kPa (Omega PX309-300G). T-type thermocouples with an accuracy of ± 0.5 °C were used to measure the temperatures. A flowmeter (Omega FTB-1300) with an accuracy of $\pm 1\%$ was also installed after the recuperator to measure refrigerant flow rate. Sight glasses were installed before the expansion valve, on the two-phase separator, and before the compressor inlet to visualize refrigerant qualities.

The phase separator used in these tests is a gravity-dependent separator that buoyantly separates the liquid and vapor phases based on their density difference. The separator consists of a two-phase inlet, a vapor outlet at the top, and a liquid outlet located opposite to the two-phase inlet. A sight glass was installed on the side wall of the phase separator chamber at about the same height as the liquid outlet tubing to visualize the liquid level. By adjusting the pressure drop through a metering valve located on the top of the phase separator, a stable liquid level in the phase separator was maintained at the height of the sight glass and effectively separated the liquid and vapor phases.

A recuperator (also known as a liquid suction heat exchanger) was used to exchange heat between the hot liquid from the condenser and the cold vapor (or two-phase mixture) that exited from the evaporator. With the recuperator, the liquid was subcooled before it entered the expansion valve which reduced the vapor quality after the expansion valve. In addition, the recuperator was used to evaporate any residual liquid that may exit the evaporator to ensure that only vapor entered the compressor.

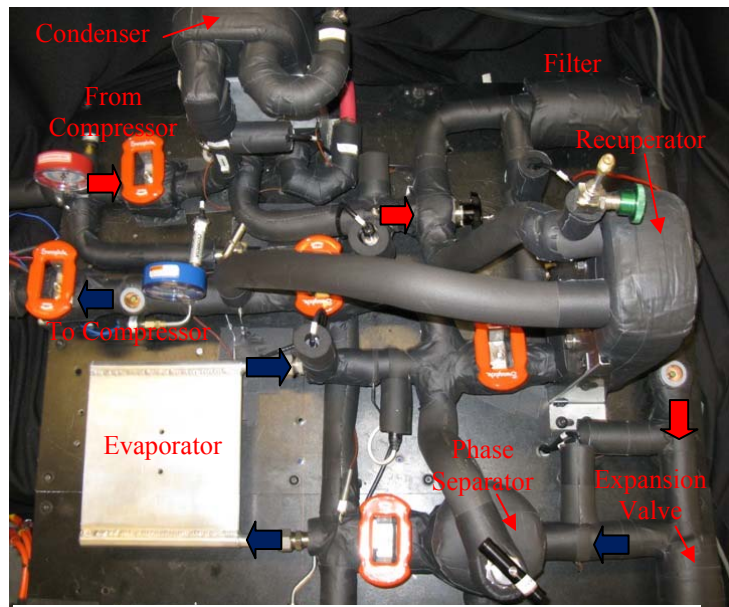


FIGURE 5. VCL test bed with phase separator and recuperating heat exchanger (recuperator).

Two heating plates, each with eight cartridge heaters, were clamped to the 20.3cm x 20.3cm evaporator surfaces and used as a controlled heat source (Figure 6). A graphite pad (Graph Tech HT-1210) was inserted between the heater plates and the evaporator and thermal grease (OmegaTherm 201) was used between the evaporator tubes and the saddle shape aluminum plates to minimize interfacial thermal resistance. Six thermocouples were installed on each side of the heating plate and their locations are indicated with “x” in Figure 6.

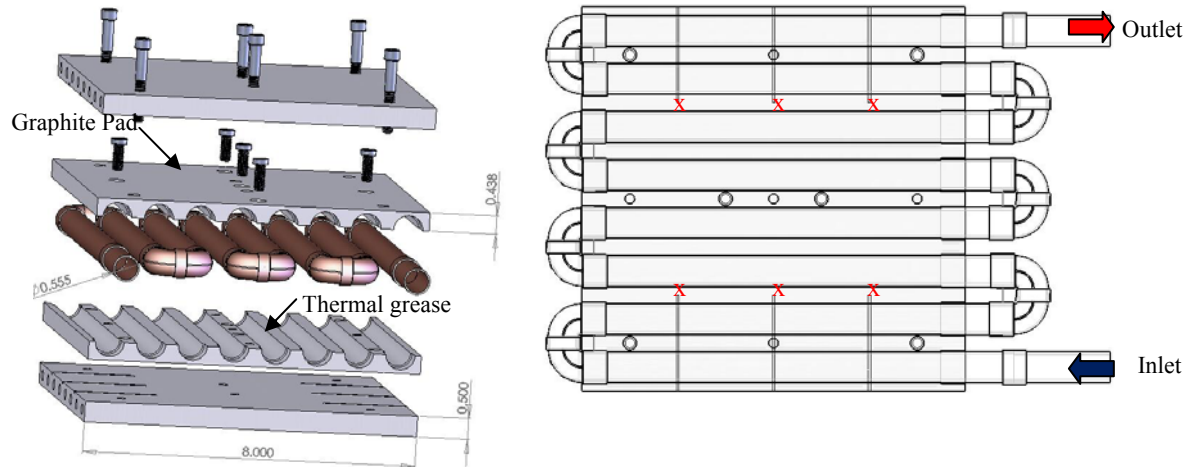


FIGURE 6. Evaporator E1 assembly with heaters (left) and evaporator thermocouple location (right).

Tests were performed at different heat loads using R134a refrigerant. In all tests, the condenser coolant inlet temperature was maintained at 45°C. Two different feedback methods to control the refrigerant flow rate were evaluated. The evaporator E1 was used for these tests. The first method (*Method A*) monitored the superheat at the evaporator exit while the second method (*Method B*) monitored the superheat at the recuperator exit. Both methods adjusted the refrigerant flow rate in response to the temperature, which varied as a function of the heat load, and maintained a constant superheat. During initial baseline tests, *Method A* resulted in the production of superheated vapor in part of the evaporator. Since the single-phase heat transfer coefficient for superheated vapor is a fraction of the two-phase heat transfer coefficient, the evaporator temperature was nonuniform. As result, *Method B* was developed to ensure that two-phase flow was present throughout the entire evaporator length and the production of the superheated vapor occurred in the recuperator. More uniform evaporator temperatures have been demonstrated using *Method B*.

RESULTS

The refrigerant temperatures for evaporator E1 at different heat loads using *Method A* superheat control are given in Figure 7. It can be seen that all loop temperatures were steady with the exception of the evaporator outlet temperature. The evaporator outlet temperature was affected by cyclic opening/closing of the expansion valve. It can also be observed from Figure 7, that the recuperator subcooled the hot liquid from the condenser and superheated the vapor from the evaporator.

The maximum and minimum heater surface temperatures using *Method A* and *Method B* are shown in Figure 8. The key difference between the two methods was that when using *Method B*, the refrigerant mass flow rate was increased resulting in a two-phase mixture at the evaporator exit.

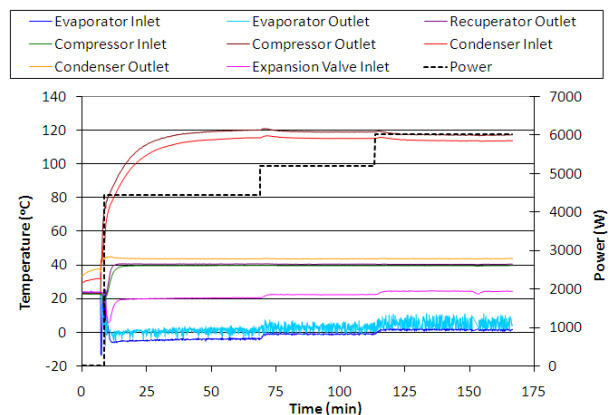


FIGURE 7. Refrigerant temperatures at different locations of the VCL test bed using *Method A* superheat control.

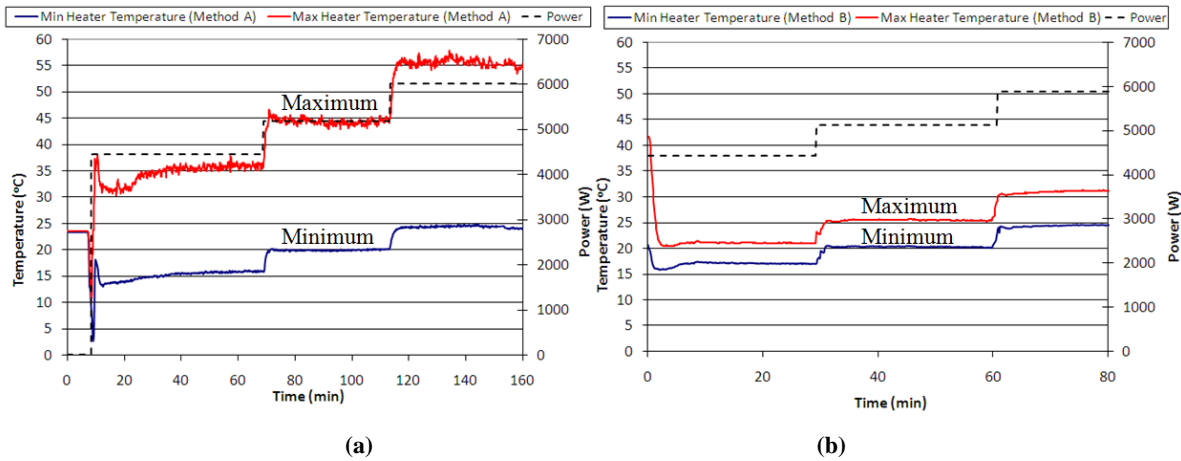


FIGURE 8. Minimum and maximum heater surface temperatures using (a) Method A with a low refrigerant flow rate and (b) Method B with a high refrigerant flow rate for evaporator E1.

Figure 8 indicates that when using *Method A* the heater surface temperature is less uniform as compared to *Method B*. The large temperature non-uniformity for *Method A* is a result of the low heat transfer coefficient associated with the flow of superheated vapor. The average heat transfer coefficient for a phase change of the R134a was determined to be $\sim 6000 \text{ W/m}^2\text{K}$ while the heat transfer coefficient of the superheated vapor was calculated to be $\sim 280 \text{ W/m}^2\text{K}$. This 20-fold reduction in heat transfer accounted for the non-uniform temperature distribution on the evaporator surface when using *Method A*. In the second case, when using *Method B*, the two-phase mixture exited the evaporator. The two-phase mixture/ saturated vapor then entered the recuperator where it was superheated before it entered the compressor. At the same time, the high temperature liquid from the condenser was subcooled in the recuperator.

Relatively high temperature differences between the heater surface and the refrigerant (comparing Figure 7 and Figure 8) can also be attributed to the low thermal conductivity of the thermal interface materials (thermal grease and graphite thermal pad) compared to bulk thermal conductivities of copper and aluminum.

A comparison of the test results between *Method A* and *Method B* for evaporator E1 at a heat load of 5.9kW is summarized in Table 5 where it is noted that the refrigerant flow rate for *Method B* was higher than for *Method A*.

Table 5. Comparison of test results for Evaporator E1 using *Method A* and *Method B*

Test Method	Mass Flow Rate (kg/hr)	Heat Load (W)	Base Heat Flux (W/cm^2)	Heater Surface Temp. ¹ ($^{\circ}\text{C}$)	Evaporator Thermal Resistance ($^{\circ}\text{C-cm}^2/\text{W}$)	Temp. Lift ² ($^{\circ}\text{C}$)	COP ³
A	124.1	5867	7.1	36 \pm 13	3.2	20.2	1.8
B	152.5	5875	7.1	27 \pm 2	2.4	29.2	1.8

¹ Note that the high heater surface temperature is a result of different evaporator layers and thermal interface materials that were used to simplify testing of different evaporators.

² Difference between evaporator wall temperature and average condenser coolant temperature.

³ Coefficient of Performance (COP) is defined as the ratio of heat load and the compressor work.

The base heat flux from the heater plates, q , is also reported and was calculated as the heat load divided by the total evaporator area, 826 cm^2 . Heater surface temperatures were lower and more uniform when using *Method B*. The temperature non-uniformity was $\pm 13^{\circ}\text{C}$ for *Method A* and $\pm 2^{\circ}\text{C}$ for *Method B*. The evaporator surface temperature, T_{EW} , was calculated from measured heater surface temperature by subtracting temperature differences across the graphite pad. The evaporator thermal resistance, R_{ev} , was calculated as:

$$R_{ev} = \frac{(T_{EW} - T_{ref,average})}{q} \quad (6)$$

where $T_{ref,average}$ is the refrigerant temperature calculated as the average between refrigerant inlet and outlet temperatures. We can see that the thermal resistance for *Method B* is lower than for *Method A*. Temperature lift was calculated as a difference between evaporator surface temperature and average condenser coolant temperature. *Method B* resulted in 9°C higher temperature lift than *Method A*. The Coefficient of Performance, COP, was calculated as the ratio of the heat load and the compressor work. The COP for both methods was 1.8.

Method B was used to test evaporators E1 to E6. The evaporators were tested with and without phase separation upstream of the evaporators at different heat loads from 3-6kW. Comparison of the test results for evaporators E1 to E6 tested at a heat load of 4kW without the phase separator is given in Table 6.

Table 6. Summary of test results for evaporators E1 to E6

Category	E1	E2	E3	E4	E5	E6
Evaporator thickness (cm)	2.2	2.2	2.2	2.2	1.3	1.0
Evaporator mass (kg)	2.5	2.8	2.9	3.2	1.3	1.1
Heat load (W)	4000	4000	4000	4017	3998	3995
Base heat flux (W/cm ²)	4.8	4.8	4.8	4.9	4.8	4.8
Refrigerant mass flow rate (kg/hr)	95.5	100.1	96.9	109.7	101.9	101.5
Ave. condenser coolant temp. (°C)	45.1	45.0	45.3	45.6	45.4	45.0
Ave. refrigerant temp. in evap. (°C)	-7.6	-7.4	-6.9	-5.3	-7.5	-6.0
Ave. evap. surface temp. (°C)	12.6	7.8	3.8	5.5	8.8	8.3
Max evap. surface ΔT (°C)	3.2	4.3	4.4	2.8	9.6	12.2
Thermal resistance (°C-cm ² /W)	4.18	3.16	2.22	2.21	3.37	2.94
Temp. lift (°C)	32.5	37.2	41.5	40.1	36.5	36.7
COP	1.4	1.3	1.4	1.2	1.3	1.3
Evaporator pressure drop (kPa)	13.8	19.5	28.6	52.9	8.6	56.6

When comparing results for serpentine tube evaporators (E1 to E4), we can see that the evaporator E3 results in the lowest evaporator (and heater) temperature and the evaporator E1 results in the highest temperature. Consequently, the temperature lift for the evaporator E3 is the highest and the temperature lift for the evaporator E1 is the lowest. Evaporator E3 removed heat at one half of the thermal resistance of the baseline evaporator E1. The compressor energy consumption for both evaporators was the same. Maximum temperature difference on evaporator surface for evaporator E4 is only 2.8°C (±1.4°C) indicating very good temperature uniformity across the evaporator surface.

Evaporators E5 and E6 are more compact than the evaporators E1 to E4. For example mass of the evaporator E6 is only one third of the mass of the evaporator E4. However, the temperature uniformity for the evaporators E5 and E6 is not as good as for the evaporators E3 and E4. Thermal resistance of the evaporator E6 is lower than for the evaporators E1, E2 and E5, but it is higher than for the evaporators E3 and E4. Evaporator E5 has only slightly higher mass than evaporator E6, however, it has better temperature uniformity than evaporator E6. Thermal resistance for evaporator E5 is higher than for evaporator E6, but it is still lower than for the baseline evaporator E1.

For all the evaporators, the tests were also performed with the phase separator upstream of the evaporator. No improvements in temperature uniformity or average evaporator surface temperature were seen. It is believed that if the recuperator would not subcool the liquid before the expansion valve, the vapor quality at the evaporator inlet would be significantly higher. High vapor quality at the inlet to the parallel channel evaporators would result in maldistribution of phases into the channels and consequently very large temperature difference across the evaporator.

Evaporator thermal resistances at different heat fluxes are plotted in Figure 9. It could be seen that evaporators E3 and E4 perform significantly better than other evaporators at low heat fluxes. There is slightly less advantage at high heat fluxes. The third best is evaporator E6 and then follow evaporators E2, E5, and E1.

Evaporators E3 and E5 should be considered for Lunar Lander and Lunar Habitat electronics cooling applications due to superior performance (E3) and low evaporator mass (E5). Future work will further improve evaporator designs E3 and E5.

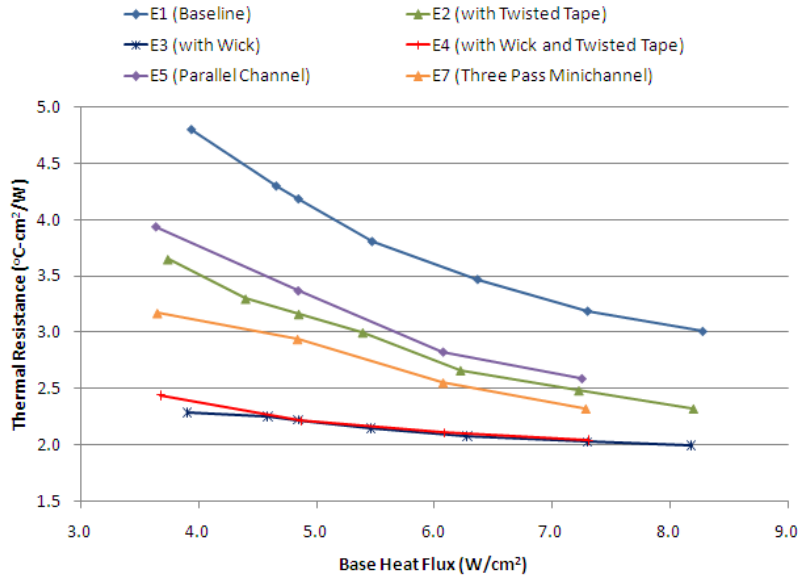


FIGURE 9. Evaporator thermal resistance as a function of base heat flux for evaporators E1 to E6.

CONCLUSIONS

Six different evaporators for Lunar Lander and Lunar Surface Systems were designed, fabricated and tested in a Vapor Compression Loop test bed for heat loads in the range of 3-6kW. The evaporators were relatively small with heated area of 826cm². The mass of the evaporators ranged from 1.0 to 3.2kg depending on the design. The objective of this work was to quantify the heat transfer characteristics of different evaporator designs and to identify the evaporator design that results in most uniform evaporator temperature, the lowest evaporator surface temperature, the lowest evaporator pressure drop, and has the lowest evaporator mass. The results obtained to date with the serpentine evaporators show excellent temperature uniformity ($\pm 3^{\circ}\text{C}$) across the evaporator surface for heat loads up to 6kW. The temperature lift from the evaporator wall to the average condenser coolant temperature was also measured and ranged from 30 to 50°C depending on the heat load and the evaporator design. The Coefficient of Performance (COP) at 6kW was 1.9. The serpentine evaporator with wick and the parallel channel evaporator appear to be the most promising for Lunar Landers and Lunar Habitats due to superior performance and low evaporator mass. The following could be concluded for this work:

- Non-conventional refrigerant flow control based on feedback from the temperature of the superheated vapor at the recuperator outlet (rather than evaporator outlet) can significantly improve the isothermality of the evaporator needed for cooling electronics components.
- The serpentine evaporator with wick (E3) and the parallel channel evaporator (E5) should be considered for Lunar Lander and Lunar Habitat electronics cooling applications.
- Future work will further minimize evaporator E3 mass and further improve temperature uniformity for evaporator E5.

NOMENCLATURE

c_{pf} = specific heat of fluid phase (J/kg K)
 d_h = hydraulic diameter (cm)
 F = Reynolds number factor (unitless)
 f_{tp} = two-phase friction factor (unitless)
 G = mass flux (kg/m²s)
 h_{fg} = latent heat of vaporization (kJ/kg)
 k_f = thermal conductivity of fluid (W/m K)
 L = evaporator length (cm)

P = pressure (kPa)
 q = heat flux into a flat evaporator (W/cm²)
 q_w = wall heat flux into refrigerant (W/cm²)
 S = suppression factor (unitless)
 T = temperature (°C)
 v_g = specific volume of vapor (m³/kg)
 v_f = specific volume of liquid (m³/kg)
 x = vapor quality (unitless)

η_f = viscosity of fluid phase (Pa s)
 ρ_{fp} = two-phase density (kg/m^3)

y = twist ratio (unitless)
 δ = thickness of twisted tape (m)

ACRONYMS

TCS – Thermal Control System
LSS – Lunar Surface Systems
VCL – Vapor Compression Loop

ACKNOWLEDGMENTS

This work was performed under a NASA SBIR Phase II program (Contract No.: NNC08CA28C). The program technical monitor was Mr. Eric Sunada. The author would like to thank Dr. Howard Pearlman and Mrs. Sanjida Tamanna from ACT for their suggestions and support. Mr. Andrew Radesky and Mr. Jeff Reichl from ACT provided laboratory support.

REFERENCES

- Abu-Khader, M. M., “Further understanding of twisted tape effects as tube insert for heat transfer enhancement,” *Heat Mass Transfer*, **43**, (2006), pp. 123-134.
- Agostini, B., Thome, J. R., Fabbri, M., Michael, B., Calmi, D. and Kloter, U., “High heat flux flow boiling in silicon multi-microchannels-Part I: Heat transfer characteristics of refrigerant R236fa,” *International Journal of Heat and Mass Transfer* **51**, (2008), pp. 5400-5414.
- Chen, J. C., “A correlation for boiling heat transfer to saturated fluid in convective flow,” *ASME Paper*, 63-HT-34, (1963), pp. 1-11.
- Ewert, M., “Investigation of lunar base thermal control system options,” *23th International Conference on Environmental Systems*, Colorado Springs, Colorado, July 12~15, (1993).
- Ganapathi, G. B., Sunada, E. T., Birur, G. C. and Miller, J. R., “Design Description and Initial Characterization Testing of an Active Heat Rejection Radiator with Digital Turn-Down Capability,” *SAE ICES*, Paper 2009-01-2419, (2009).
- Greco A. and Vanoli, G. P., “Flow-boiling of R22, R134a, R507, R404A, and R410A inside a smooth horizontal tube,” *International Journal of Refrigeration*, **28**, (2005), pp. 872-880.
- Kattan, N., Thome, J. R. and Favrat, D., “Flow Boiling in Horizontal Tubes: Part 1: Development of diabatic 2Ø flow pattern map,” *Journal of Heat Transfer* **120**, (1998), pp. 130-147.
- Manglik, R. M., and Bergels, A. E., “Heat transfer and pressure drop correlations for twisted tape inserts in isothermal tubes. Part 1: laminar flows,” *Trans. ASME J. Heat Transfer*, **116**, (1993), pp. 881-889.
- Simonsen, L. C., DeBarro, M. J. and Farmer, J. T., “Conceptual design of a lunar base thermal control system,” *2nd Conference on Lunar Bases and Space Activities of the 21st Century*, edited by W., W., Mendel, April 5-7, Houston, TX, (1988), pp. 579-591. [NASA Conference Publication 3166, 1992]
- Sridhar, K., R. and Gottmann, M., “Lunar base thermal control systems using heat pumps,” *Acta Astronautica*, **39**(5), (1996), pp. 381-394.
- Stephen, R. A., “Overview of NASA’s Thermal Control System Development for Exploration Project,” *SAE ICES*, Paper 2009-01-2436, (2009).
- Sun, L. and Mishima, K., “Evaluation analysis of prediction methods for two-phase flow pressure drop in mini-channels,” *International Journal of Multiphase Flow*, **35**, (2009), pp. 47-54.
- Swanson T., Radermacher R., Costello F., Moore J., and Mengers D., “Low-temperature thermal control for a lunar base,” *20th Intersociety Conference on Environmental Systems*, Williamsburg, Virginia, July 9-12, (1990).
- Tran, T. N., Chyu, M. C., Wambsgans, M. W. and France, D. M., “Two-phase pressure drop of refrigerants during flow boiling in small channels: an experimental investigation and correlation development,” *International Journal of Multiphase Flow*, **26**, (1999), pp.1739-1754.
- Zhang, W., Hibiki, T. and Mishima, K., “Correlation for flow boiling heat transfer in mini-channels,” *International Journal of Heat and Mass Transfer*, **47**, (2004), pp. 5749-5763.
- Yu, M., Lin, T. and Tseng, C., “Heat transfer and flow pattern during two-phase flow boiling of R-134a in horizontal smooth and microfin tubes,” *International Journal of Refrigeration*, **25**, (2002), pp.789-798.